Transition of $\rho \to \pi\gamma$ in lattice QCD

Benjamin J. Owen,[1,*] Waseem Kamleh,[1] Derek B. Leinweber,[1] M. Selim Mahbub,[1,2] and Benjamin J. Menadue[1,3]

[1]*Department of Physics, Special Research Centre for the Subatomic Structure of Matter (CSSM),*
University of Adelaide, South Australia 5005, Australia
[2]*Digital Productivity Flagship, CSIRO, 15 College Road, Sandy Bay, TAS 7005, Australia*
[3]*National Computational Infrastructure (NCI), Australian National University,*
Australian Capital Territory 0200, Australia

With the ongoing experimental interest in exploring the excited hadron spectrum, evaluations of the matrix elements describing the formation and decay of such states via radiative processes provide us with an important connection between theory and experiment. In particular, determinations obtained via the lattice allow for a direct comparison of QCD expectation with experimental observation. Here we present the first light-quark determination of the $\rho \to \pi\gamma$ transition form factor from lattice QCD using dynamical quarks. Using the PACS-CS $2 + 1$ flavor QCD ensembles we are able to obtain results across a range of masses, to the near physical value of $m_\pi = 156$ MeV. An important aspect of our approach is the use of variational methods to isolate the desired QCD eigenstate. For low-lying states, such techniques facilitate the removal of excited state contributions. In principle, the method enables one to consider arbitrary eigenstates. We find our results are in accord with the nonrelativistic quark model for heavy masses. In moving towards the light-quark regime we observe an interesting quark mass dependence, contrary to the quark model expectation. Comparison of our light-quark result with experimental determinations highlights a significant discrepancy suggesting that disconnected sea-quark loop contributions may play a significant role in fully describing this process.

I. INTRODUCTION

In the search for a complete understanding of the hadron spectrum, hadronic transitions provide a crucial dialogue between experiment and lattice QCD. Experimental programs such as those at JLAB and Mainz are producing large bodies of high-quality data [1] providing valuable insight into the underlying structure and dynamics of hadronic excitations. Meanwhile, significant effort by the lattice community has seen remarkable progress in understanding and mapping out the hadron spectrum from the perspective of QCD [2,3]. Having isolated such states, evaluations of their transition form factors provide crucial insight into their production mechanisms allowing for direct comparison between QCD and the experimental observations. Another exciting prospect is that lattice determinations may help in the experimental search for as yet unseen QCD eigenstates, such as exotic hadron states being sought by the GlueX experiment [4].

Among the simplest radiative process that can be examined on the lattice is the radiative decay of the rho meson into a pion. This process is described by a single form factor, $G_{M1}(Q^2)$, and as both states are the lowest lying single particle states in their respective channels, extraction is relatively simple. Evaluations of this transition were considered early in the course of lattice structure calculations, first by Woloshyn [5] and later by Lubicz and Crisafulli [6]. More recently, our preliminary study [7] examined both the ρ and K^* transition form factors down to lighter masses ($m_\pi \simeq 300$ MeV). However, all of these studies used quenched gauge field configurations. Currently the only evaluations in full QCD are those of Edwards [8] and Shultz [9] in which this transition along with a range of other elastic and transitions form factors were considered. However, the parameters considered were far from physical, particularly the large pion mass. There is thus a need to examine this transition at light-quark masses using dynamical quarks.

Recently the issue of excited states has received renewed focus [10–12] as lattice determinations of several quantities, most notably the nucleon axial charge, g_A, and quark momentum fraction, $\langle x \rangle$, continue to differ systematically from the experimental results despite operating at near physical quark masses and large lattice volumes. In Refs. [13,14], we presented a framework for utilizing variational techniques for the extraction of hadronic matrix elements. For both the calculation of g_A [13] and the electromagnetic form factors of the π and ρ mesons [14], we found that the use of correlation matrix methods led to significantly improved ground state dominance over the standard single smeared source approach. This in turn allowed for the use of earlier current insertion times and subsequently consider earlier fit windows resulting in improved statistical uncertainties. Furthermore, within

*benjamin.owen@adelaide.edu.au

Ref. [14] we were able to examine the corresponding matrix elements for both excited pi and rho meson states. The same techniques were utilized by Shultz *et al.* [9] to examine the transition form factors for the lightest π and ρ excited states. In this work we will make use of such techniques in our determination of the $\rho \to \pi\gamma$ transition form factors across a wide range of quark masses including the light-quark regime.

The remainder of this investigation is organized as follows. In Sec. II we present a brief summary of the use of variational methods in the evaluation of transition matrix elements. Section III outlines how we intend to extract the transition form factor, $G_{M1}(Q^2)$ and finally a summary of calculation details in Sec. IV. Our results are discussed in Sec. V followed by concluding remarks in Sec. VI.

II. CORRELATION MATRIX METHODS FOR HADRON TRANSITIONS

The use of variational techniques for the calculation of hadronic matrix elements has been presented in Refs. [13,14] and here we present a brief outline to define our procedure and notation. Similar prescriptions have been explored in Refs. [15–20]. The variational method [21,22] is an approach to generating a set of ideal operators, $\{\phi^\alpha\}$, constructed to have overlap with an individual eigenstate

$$\langle\Omega|\phi^\alpha|\beta, p\rangle \propto \delta^{\alpha\beta}. \tag{1}$$

This is achieved by choosing an existing basis of operators, $\{\chi_i\}$, and constructing these idealized operators as linear combinations

$$\phi^\alpha(x) = \sum_i v_i^\alpha \chi_i(x), \qquad \phi^{\alpha\dagger}(x) = \sum_j \chi_j^\dagger(x) u_j^\alpha. \tag{2}$$

Starting from the matrix of two-point correlation functions

$$G_{ij}(\vec{p}, t) = \sum_{\vec{x}} e^{-i\vec{p}\cdot\vec{x}} \langle\Omega|\chi_i(x)\chi_j^\dagger(0)|\Omega\rangle,$$

one can show that both $v_i^\alpha G_{ij}(\vec{p}, t + \delta t)$ and $G_{ij}(\vec{p}, t + \delta t) u_j^\alpha$ provide a recurrence relation from which the necessary vectors, v_i^α and u_j^α, are the solutions of the following generalized eigenvalue equations

$$v_i^\alpha G_{ij}(\vec{p}, t_0 + \delta t) = e^{-E_\alpha(\vec{p})\delta t} v_i^\alpha G_{ij}(\vec{p}, t_0) \tag{3a}$$

$$G_{ij}(\vec{p}, t_0 + \delta t) u_j^\alpha = e^{-E_\alpha(\vec{p})\delta t} G_{ij}(\vec{p}, t_0) u_j^\alpha. \tag{3b}$$

With the optimized operator for the state $|\alpha, p\rangle$ suitably defined, one can construct the corresponding correlator by projecting the matrix of correlators

$$G(\vec{p}, t; \alpha) = (v(\vec{p}))_i^\alpha G_{ij}(\vec{p}, t)(u(\vec{p}))_j^\alpha.$$

Here we note that the correlators that feed into Eq. (3a) and (3b) are functions of the 3-momentum, $\vec{p}$. Therefore it is necessary to evaluate eigenvectors for each momentum considered. This is of particular relevance to three-point correlators where the incoming and outgoing momenta in general differ.

To obtain the three-point correlator necessary for describing a particular transition, it is a simple matter of projecting the relevant states with the corresponding eigenvectors for source and sink. In order to do this, one first evaluates the matrix of three-point correlation functions required for the transition in question

$$(G_{\mathcal{O}}^{a\to b})_{ij}(\vec{p}', \vec{p}, t_2, t_1)$$
$$= \sum_{\vec{x}_2, \vec{x}_1} e^{-i\vec{p}'\cdot(\vec{x}_2-\vec{x}_1)} e^{-i\vec{p}\cdot\vec{x}_1} \langle\Omega|\chi_{b,i}(x_2)\mathcal{O}(x_1)\chi_{a,j}^\dagger(0)|\Omega\rangle, \tag{4}$$

where $\mathcal{O}$ is the current operator through which the transition takes place and the labels a and b highlight that the source and sink operators can correspond to different J^{PC}. In this situation, one must construct ideal operators for each set of quantum numbers. By performing the variational analysis with the bases $\{\chi_{a,i}\}$ and $\{\chi_{b,i}\}$, we obtain two sets of eigenvectors: $(v_a)_i^\alpha$, $(u_a)_j^\alpha$ and $(v_b)_i^\beta$, $(u_b)_j^\beta$ which form optimized operators of type a and b, respectively. It is then a simple matter of projecting the necessary eigenvectors onto the matrix of three-point functions, where care is taken to ensure that the projection is done with the correct momenta and operator for source and sink

$$G_{\mathcal{O}}^{a\to b}(\vec{p}', \vec{p}, t_2, t_1; \beta, \alpha)$$
$$\equiv (v_b(\vec{p}'))_i^\beta (G_{\mathcal{O}}^{a\to b})_{ij}(\vec{p}', \vec{p}, t_2, t_1)(u_a(\vec{p}))_j^\alpha.$$

Having acquired the projected two and three-point correlation functions, determination of matrix elements then follows in the standard way through the construction of a suitable ratio. For transitions, we choose to work with a modified form of the ratio presented in Ref. [23]

$$R(p', p; \beta, \alpha)$$
$$= \sqrt{\frac{\langle G_{\mathcal{O}}^{a\to b}(\vec{p}', \vec{p}, t_2, t_1; \beta, \alpha)\rangle\langle G_{\mathcal{O}}^{b\to a}(\vec{p}, \vec{p}', t_2, t_1; \alpha, \beta)\rangle}{\langle G_a(\vec{p}, t_2; \alpha)\rangle\langle G_b(\vec{p}', t_2; \beta)\rangle}}. \tag{5}$$

Though this requires the evaluation of both $+\vec{q}$ and $-\vec{q}$ sequential source technique (SST) propagators [24,25], if one wishes to use both $\{U\}$ and $\{U^*\}$ configurations as was done in Refs. [14,26] and will be done here, then these are required regardless of the choice of ratio [27].

III. $\rho \to \pi\gamma$ TRANSITION FORM FACTORS

Having outlined the method for obtaining the projected correlators and the corresponding ratios, we now consider how to isolate the form factor describing the radiative decay of the rho meson. In order to do so we make the identification that $a = \pi$, $b = \rho$ and $\mathcal{O} = J^\mu$ the electromagnetic current. For this discussion we shall work with the standard Minkowski metric. Starting from the projected three-point correlation function

$$
(G_{\rho \to \pi\gamma})^\mu_\nu(\vec{p}, \vec{p}', t_2, t_1; \alpha, \beta)
$$
$$
= \sum_{\vec{x}_2, \vec{x}_1} e^{-i\vec{p}\cdot(\vec{x}_2 - \vec{x}_1)} e^{-i\vec{p}'\cdot\vec{x}_1} \langle\Omega|\phi_\pi^{\alpha,\vec{p}}(x_2) J^\mu(x_1) \phi_{\rho,\nu}^{\beta,\vec{p}'\,\dagger}(0)|\Omega\rangle,
$$

$$(6)$$

we begin by inserting completeness identities between our operators in order to obtain the desired matrix element, as well as operator overlap factors. This matrix element, which describes the transition, can be parametrized by a single form factor G_{M1}

$$
\langle\pi_\alpha(\vec{p})|J^\mu(0)|\rho_\beta(\vec{p}', s')\rangle
$$
$$
= \frac{1}{2\sqrt{E_{\pi_\alpha}(\vec{p}) E_{\rho_\beta}(\vec{p}')}} \left(\frac{-ie}{m_{\rho_\beta}}\right) G_{M1}(Q^2) \varepsilon^{\mu\delta\sigma\tau} p'_\delta p_\sigma \epsilon_\tau^\beta(p', s'),
$$

$$(7)$$

where we note that our choice of normalization is that of Ref. [5]. Furthermore we note the pion overlap can be expressed as

$$
\langle\Omega|\phi_\pi^{\alpha,\vec{p}}(0)|\pi_\beta(\vec{p})\rangle = \frac{\delta^{\alpha\beta}}{\sqrt{2E_{\pi_\alpha}(\vec{p})}} \mathcal{Z}_\pi^\alpha(\vec{p})
$$

and similarly the rho meson overlap

$$
\langle\Omega|\phi_{\rho,\nu}^{\alpha,\vec{p}}(0)|\rho_\beta(\vec{p}, s)\rangle = \frac{\delta^{\alpha\beta}}{\sqrt{2E_{\rho_\alpha}(\vec{p})}} \epsilon_\nu^\alpha(p, s) \mathcal{Z}_\rho^\alpha(\vec{p})
$$

where $\epsilon(p, s)$ is a spin polarization vector which satisfies

$$
\sum_s \epsilon_\mu(p, s) \epsilon_\nu^*(p, s) = -\left(g_{\mu\nu} - \frac{p_\mu p_\nu}{m_{\rho_\alpha}}\right).
$$

Substituting these expressions into Eq. (6) and making use of the spin-sum identity we arrive at

$$
(G_{\rho \to \pi\gamma})^\mu_\nu(\vec{p}, \vec{p}', t_2, t_1; \alpha, \beta) = \frac{e^{-E_{\pi_\alpha}(\vec{p})(t_2 - t_1)} e^{-E_{\rho_\beta}(\vec{p}')t_1}}{4E_{\pi_\alpha}(\vec{p}) E_{\rho_\beta}(\vec{p}')} \mathcal{Z}_\pi^\alpha(\vec{p}) \mathcal{Z}_\rho^{\beta\,\dagger}(\vec{p}') \left(\frac{+ie}{m_{\rho_\beta}}\right) G_{M1}(Q^2) \varepsilon^{\mu\delta\sigma\tau} p'_\delta p_\sigma \left(g_{\tau\nu} - \frac{p'_\tau p'_\nu}{m_{\rho_\beta}^2}\right).
$$

Our construction of the ratio of three- and two-point functions in Eq (5) requires the consideration of both $\rho \to \pi\gamma$ and $\pi\gamma \to \rho$ in extracting the form factors. While both time-orderings are considered, the freedom to attribute a unique momentum to each meson remains. Taking the Hermitian conjugate of Eq. (7), we can obtain the time-reversed matrix element necessary for $G_{\pi\gamma \to \rho}$. Following the same procedure we arrive at the corresponding expression

$$
(G_{\pi\gamma \to \rho})^\mu_\nu(\vec{p}', \vec{p}, t_2, t_1; \beta, \alpha) = \frac{e^{-E_{\rho_\beta}(\vec{p}')(t_2 - t_1)} e^{-E_{\pi_\alpha}(\vec{p})t_1}}{4E_{\pi_\alpha}(\vec{p}) E_{\rho_\beta}(\vec{p}')} \mathcal{Z}_\rho^\beta(\vec{p}') \mathcal{Z}_\pi^{\alpha\dagger}(\vec{p}) \left(\frac{-ie}{m_{\rho_\beta}}\right) G_{M1}(Q^2) \varepsilon^{\mu\delta\sigma\tau} p'_\delta p_\sigma \left(g_{\tau\nu} - \frac{p'_\tau p'_\nu}{m_{\rho_\beta}^2}\right).
$$

In order to cancel out the time dependence and the overlap factors, $\mathcal{Z}$, we require the projected two-point functions

$$
G_\pi(\vec{p}, t_2; \alpha) = \sum_{\vec{x}_2} e^{-i\vec{p}\cdot\vec{x}_2} \langle\Omega|\phi_\pi^{\alpha,\vec{p}}(x_2) \phi_\pi^{\alpha,\vec{p}\,\dagger}(0)|\Omega\rangle
$$

$$
(G_\rho)_{\nu\nu}(\vec{p}', t_2; \beta) = \sum_{\vec{x}_2} e^{-i\vec{p}'\cdot\vec{x}_2} \langle\Omega|\phi_{\rho,\nu}^{\beta,\vec{p}'}(x_2) \phi_{\rho,\nu}^{\beta,\vec{p}'\,\dagger}(0)|\Omega\rangle,
$$

where we note that repeated indices are not summed over. Again applying completeness and replacing spin-sums, these expressions reduce to

$$
G_\pi(\vec{p}, t_2) = \frac{e^{-E_{\pi_\alpha}(\vec{p})t_2}}{2E_{\pi_\alpha}(\vec{p})} \mathcal{Z}_\pi^\alpha(\vec{p}) \mathcal{Z}_\pi^{\alpha\dagger}(\vec{p})
$$

$$
(G_\rho)_{\nu\nu}(\vec{p}', t_2) = -\frac{e^{-E_{\rho_\beta}(\vec{p}')t_2}}{2E_{\rho_\beta}(\vec{p}')} \mathcal{Z}_\rho^\beta(\vec{p}') \mathcal{Z}_\rho^{\beta\dagger}(\vec{p}')
$$

$$
\times \left(g_{\nu\nu} - \frac{p_\nu p_\nu}{m_{\rho_\beta}^2}\right).
$$

Finally, substituting in the explicit form of both two and three-point correlation functions into Eq. (5), we obtain the

expression which directly relates our ratio to the form factor $G_{M1}(Q^2)$

$$R_\nu^\mu(p', p; \beta, \alpha) = \frac{e\varepsilon^{\mu\delta\sigma}{}_\nu p'_\delta p_\sigma G_{M1}(Q^2)}{2\sqrt{E_{\pi_\alpha}(\vec{p})E_{\rho_\beta}(\vec{p}')((p'_\nu)^2 - m_{\rho_\beta}^2 g_{\nu\nu})}}.$$

(8)

For our calculation we use SST propagators evaluated by fixing the current. In particular, we fix the current 3-momentum to $\vec{q} = \pm\frac{2\pi}{L}\hat{x} \equiv \pm\vec{\xi}$, the current polarization $\mu = 3$ and the vector meson polarization to be $\nu = 2$. Using these kinematics, the term $\varepsilon^{\mu\delta\sigma}{}_\nu p'_\delta p_\sigma$ reduces to $(p'_0 p_1 - p_0 p'_1)$. We choose to refine this further by taking one of the particles to be at rest. In doing so, we still have the freedom to choose which of the particles is at rest giving rise to the distinct kinematics choices: $\vec{p}' = \vec{\xi}, \vec{p} = 0$ ($\vec{q} = +\vec{\xi}$) and $\vec{p}' = 0, \vec{p} = \vec{\xi}$ ($\vec{q} = -\vec{\xi}$), each of which gives distinct values of Q^2. Applying these kinematics to Eq. (8) we arrive at the final expressions used in our evaluation of the $\rho \to \pi\gamma$ transition form factor

$$G_{M1}(Q^2) = \frac{2m_{\rho_\beta}}{e|\vec{q}|}\sqrt{\frac{E_{\rho_\beta}(\vec{q})}{m_{\pi_\alpha}}}R_2^3(\vec{\xi}, 0; \beta, \alpha)$$

$$\text{for } Q^2 = |\vec{q}|^2 - (E_{\rho_\beta}(\vec{q}) - m_{\pi_\alpha})^2;$$

$$G_{M1}(Q^2) = \frac{2m_{\rho_\beta}}{e|\vec{q}|}\sqrt{\frac{E_{\pi_\alpha}(\vec{q})}{m_{\rho_\beta}}}R_2^3(0, \vec{\xi}; \beta, \alpha)$$

$$\text{for } Q^2 = |\vec{q}|^2 - (m_{\rho_\beta} - E_{\pi_\alpha}(\vec{q}))^2,$$

where for the first expression the pion is taken to be at rest while for the second expression the ρ is at rest.

IV. SIMULATION DETAILS

For this calculation we use the PACS-CS $(2 + 1)$-flavor dynamical-QCD gauge field configurations [28] made available through the ILDG [29]. These ensembles use a nonperturbatively $\mathcal{O}(a)$-improved Wilson fermion action and Iwasaki gauge action on a $32^3 \times 64$ lattice, with periodic boundary conditions. The value $\beta = 1.9$ provides a lattice spacing of $a = 0.0907$ fm, yielding a physical box length of 2.9 fm. We have access to a total of five light-quark masses, with the strange quark mass held fixed. The resulting pion masses range from 702 down to 156 MeV. We note that when quoting results away from the physical point we set the scale using the Sommer parameter [30] with $r_0 = 0.492$ fm [28]. Due to the limited number of configurations at the lighter masses, we make use of multiple quark sources on each configuration. We also evaluate the correlators on the $\{U^*\}$ configurations through the use of the U^* trick outlined in Refs. [27,31].

For the evaluation of the three-point correlators we follow the approach where the SST propagators are evaluated with the current held fixed. For this we use a conserved vector current [26,32] with polarization $\mu = 3$ and 3-momentum transfer $\vec{q} = \pm\frac{2\pi}{L}\hat{x}$. This current is inserted at time $t_c = 21$ relative to the quark source at $t_{\text{src}} = 16$. We note that for our choice of ratio we require both $+\vec{q}$ and $-\vec{q}$; however, this is also required for the U^* trick when using SST propagators. Our error analysis is performed using a second-order jackknife, with the χ^2/dof for our fits is obtained through the covariance matrix.

As was done in Ref. [14], the antiquark contribution is evaluated through considerations of charge conjugation in order to avoid the need to evaluate backwards-propagating SST propagators. In doing so one finds that the quark sectors for the forward and backwards propagating quark fields are of equal magnitude, but differ in sign when exact isospin is present.

For the variational analysis, we use a basis of local meson operators of varying widths [33]. This is achieved by applying different levels of gauge-invariant Gaussian smearing to the quark sources and sinks. By using a variety of widths, the resulting optimized interpolators appear to form nodal structures in the radial wave-function [34]. Thus we expect our operators to have greatest overlap with states that contain dominant s-wave components. As these states are strongly peaked at the origin, we would expect these states to have the largest overlap with standard local operators and so the dominant source of excited state contamination for the standard single-source approach. The local operators we choose to use are

$$\chi_\pi(x) = \bar{d}(x)\gamma_5 u(x)$$

$$\chi_{\rho,i}(x) = \bar{d}(x)\gamma_i u(x),$$

with four different smearing widths, allowing for the construction of a 4×4 correlation matrix. The correlation-matrix analysis is performed using $t_0 = 17$ with $\delta t = 3$ for the three heavier masses and $\delta t = 2$ for the remaining two lightest masses.

V. RESULTS

Before we examine the transition form factor, we examine the isolation of the eigenstates in question. In Fig. 1 we highlight the improved ground-state dominance provided by the variational approach for the pion and ρ meson through a comparison of the time series for the effective mass extracted through the variational method and using standard smeared correlator methods. For the ρ meson the variational approach provides significant improvement allowing for significantly earlier fits due to the rapid onset of ground state dominance. In Fig. 2 we present the masses of the π and ρ mesons extracted from our variational analysis. For the lightest quark mass, which
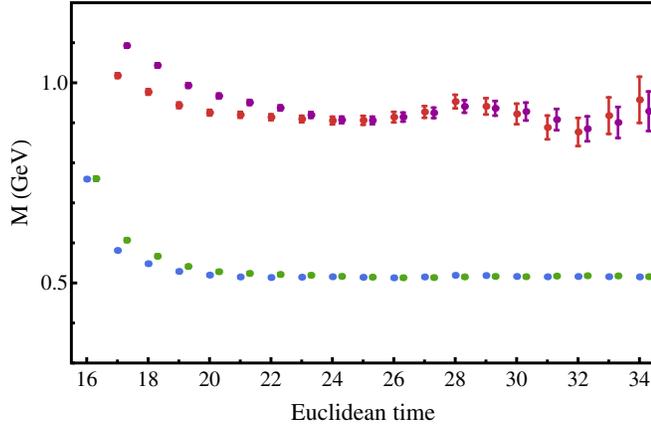
FIG. 1 (color online). Comparison of the Euclidean time series for the effective mass of the pion and ρ meson using the variational approach and standard single-source method with a moderate level of smearing (35 sweeps). The blue and green data sets are for the pion using the variational and standard approach, respectively, while the red and purple data sets are for the ρ meson using the variational and standard approach, respectively. In both cases we can see that the variational approach provides improved ground-state dominance; however, it is most notable in the case of the ρ meson where the variational result allows for fits four times slices earlier than the standard approach.

is only slightly heavier than physical, we find that both states agree well with experimental measurements. Nonetheless, for the rho meson we must take care to ensure that the state we have isolated is in fact the single particle state and not a scattering state. In Ref. [35] it was found that despite coupling poorly to local operators, scattering states can still populate the projected correlators. At early times, the weak operator coupling acts to suppress their contribution relative to the dominant single particle state. However, if the single particle state is above threshold, at large Euclidean times its contribution is suppressed
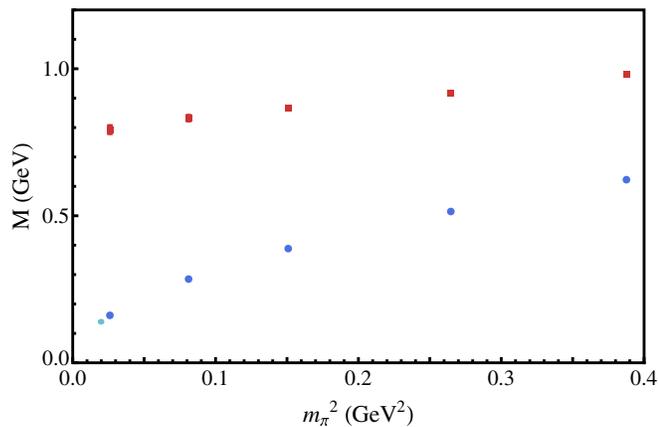
through the exponential behavior of the correlator rendering the scattering state the dominant term. There it was noted that in such a scenario, one could identify a second region of linear behavior in the logarithm of the projected correlator. We shall use this signature to identify how far we can sample the correlator and still guarantee single particle dominance. We highlight this in Fig. 3 for both the π and ρ meson, with the state at rest and boosted to $\vec{p} = \vec{q}$. We have definite liner behavior before and well after the insertion of the current.

On these ensembles the ρ meson at rest remains lighter than the nearest $\pi\pi$-scattering state; however, this is not the case for nonzero momentum. As was done in Ref. [14], we perform a detailed check of our extracted eigenstates to ensure that we have in fact isolated the single particle state. To do this we compare the extracted eigenstate energy
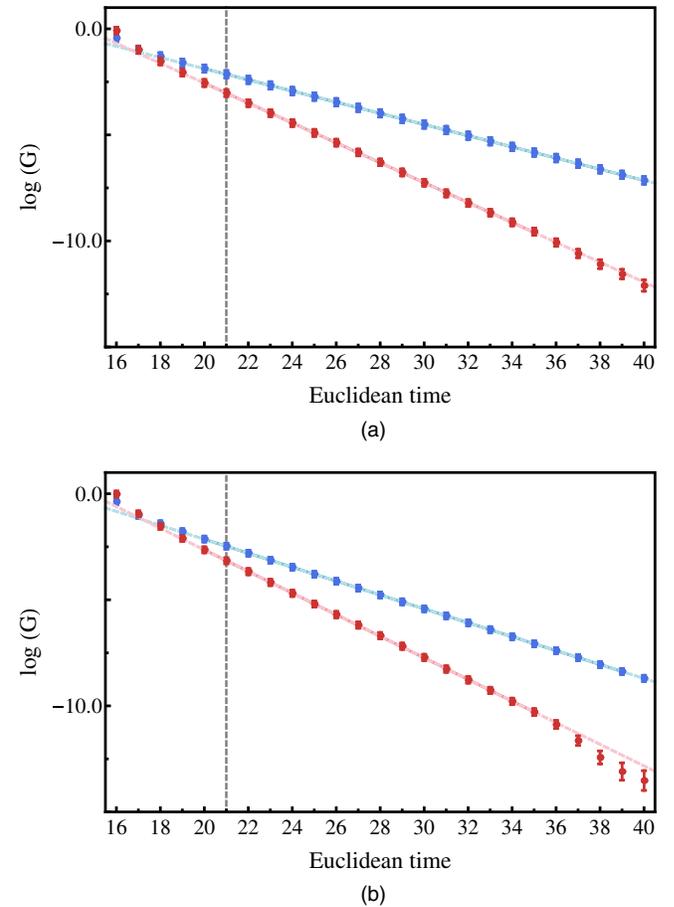

(a)

(b)

FIG. 3 (color online). Euclidean time series for $\log G$ of the π (blue) and ρ (red) mesons, obtained using the variational approach. The solid lines are the lines of best fit highlighting the timeframe over which single state dominance is observed. These lines are extended with a dashed line of the same color to highlight where the data diverges from the single state dominance. The vertical dashed lines indicate the position of the current insertion. (a) For the states at rest. (b) For the states boosted to $\vec{p} = \vec{q}$.

FIG. 2 (color online). Masses of the π (blue) and ρ (red) mesons. The lighter data points at the far left are the corresponding PDG averages [1].

against the single-particle dispersion expectation, where the mass used for the dispersion expectation is the energy extracted from the zero-momentum correlator. In Fig. 4 we demonstrate this comparison for the second lightest quark-mass considered, where we overlay the dispersion relation expectation (blue band) with the energies extracted from the finite-momentum correlators (blue data points) for a range of momenta. Here we can see excellent agreement between the extracted energies and the dispersion result. This is observed for all quark masses considered.

As a further check, we compare the extracted energies to the noninteracting $\pi\pi$ states allowed by momentum and parity conservation, indicated by the red diamonds in Fig. 4. For one unit of the lattice momentum, utilized in our form factor determinations, we observe significant mass separations between our extracted eigenstate energies and the noninteracting $\pi\pi$ energies. We further note that the attractive nature of the finite-volume interaction of the $\pi\pi$ system acts to increase the separation between the single and multiparticle dominated states on the lattice. Similar separations are found for all other masses with the exception of the middle mass where the separation is somewhat smaller.

For the particular kinematics and parameters considered in this work, we find that the determinations of G_{M1} with the pion at rest all lie below $Q^2 = 0$, while those with the rho meson at rest lie above. This gives us values for G_{M1} on either side of $Q^2 = 0$. In order to compare with experiment and quark model expectations we require a determination of $G_{M1}(0)$. To do this we choose to interpolate between our extracted values using a monopole ansatz
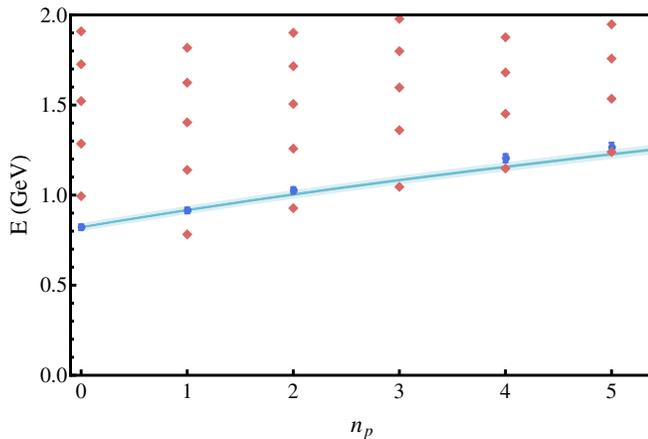

FIG. 4 (color online).   An example of our comparison between the dispersion relation $E = \sqrt{m^2 + n_p |\vec{p}_{\min}|^2}$ (blue line), and the energies extracted from the finite-momentum correlators (blue circles) for the rho meson over a range of momenta. Here m is taken from the zero-momentum correlator, $|\vec{p}_{\min}|$ is the magnitude of the lowest nontrivial momentum on the lattice. The red diamonds provide the corresponding noninteracting $\pi\pi$-energies allowed by momentum conservation. Results at the other values of m_π are similar.

$$G_{M1}(Q^2) = \left(\frac{\Lambda^2}{\Lambda^2 + Q^2}\right)G_{M1}(0). \qquad (9)$$

This choice is motivated by vector meson dominance (VMD) arguments which suggest the form factor should exhibit such a behavior in the region of low Q^2. In these models, the pole mass is identified as the vector meson, i.e. $\Lambda \simeq m_\rho$. In Ref. [6], it was found that the VMD hypothesis faired poorly with the data; however, we note that this study was conducted with rather large values of Q^2 stemming from their small lattice volume. Contrary to this, the results of Edwards [8] which examined the transition over a range of Q^2 between $0.02 - 0.6$ GeV, display behavior consistent with this expectation.

During the extraction of the quark sector contributions to the form factor, we compared the time series for the ratio using the correlation matrix approach and the standard single smeared source and sink correlator. For all masses and kinematics, we again find that the correlation matrix method improves the quality of the plateau over the single level of smearing, but not to the extent observed in previous works [13,14]. In particular, the ratio sampling in the timelike region requires significantly more Euclidean time evolution than the corresponding ratio sampling the space-like region. We note that in this case the rho meson carries the momentum and the pion is at rest. Figure 5 highlights this comparison for a single quark mass.

In Fig. 6 we present our results for the extracted values for the u-quark sector contribution to the form factor, G^u_{M1}, as well as the corresponding interpolations used to extract $G^u_{M1}(0)$. Here we choose to label these as the quark sector contributions to the positive-charge eigenstate of the corresponding iso-triplet. That is, the quark contribution is labelled as the u-quark sector while the antiquark contribution is labelled as the d-quark sector. As was mentioned in the previous section, the antiquark contribution is equal in magnitude with opposite sign, $G^d_{M1} = -G^u_{M1}$, and so we choose to show the quark contribution only. The quark sector contributions are for quarks of unit-charge. We note that the spread of Q^2 sampled is much larger in the timelike region due to the increasing Q_0-component stemming from the Goldstone nature of the pion. In the spacelike region, we see this effect is suppressed when the momentum is carried by the pion. This tight grouping of Q^2 values shows a clear decrease in the value of G^u_{M1} as the quark masses become light.

In the timelike region, the most striking feature is the significantly small value obtained for the lightest mass. However, examination of the projected two-point function appears consistent with a single particle state. We shall note that the plateau for this particular extraction of G^u_{M1} differed in nature to those at heavier masses. Based upon the χ^2_{dof}, one is able to fit much earlier; however, this is likely the result of a significant increase in the uncertainty of G^u_{M1} at
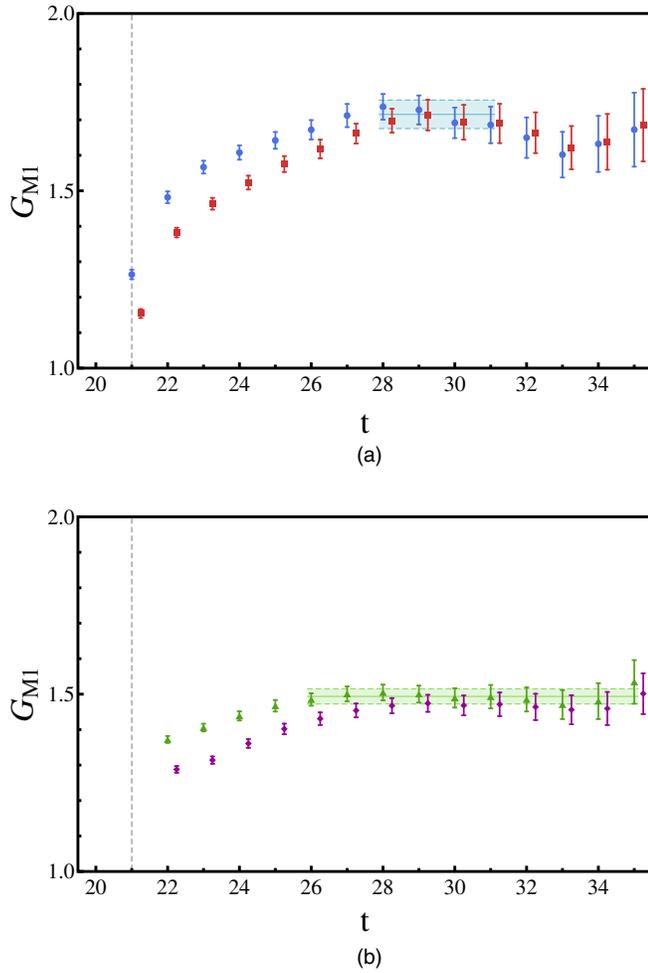
(a)

(b)

FIG. 5 (color online).   A comparison of the u-quark contribution to the transition form factor, G_{M1}^u, as a function of Euclidean sink time for a single level of smearing and our variational approach. The two data sets are offset for clarity. The upper figure is for the π meson at rest with the (blue) circles denoting the results from the variational approach while the (red) squares illustrate traditional results using the standard single-source method with a moderate level of smearing (35 sweeps). The lower figure is for the ρ meson at rest with the (green) triangles denoting the variational method and the (purple) diamonds denoting the single-source method. The vertical dashed lines indicate the position of the current insertion. The fitted value from the variational approach has been included (shaded band) to highlight where the single-source approach is consistent with our improved method. (a) G_{M1}^u with the π at rest. (b) G_{M1}^u with the ρ at rest.

early time slices. Guided by the fit windows at heavier masses we choose to fit at later times; however, it is certainly possible that we simply do not have sufficient statistics and so obtain a value for G_{M1}^u that is suppressed. Another possibility is that we are sampling too far into the timelike region for the VMD hypothesis to hold. Therefore this result may suggest that this process is suppressed at large timelike momentum transfers. As a check of the potential impact that this may have on the extracted value of
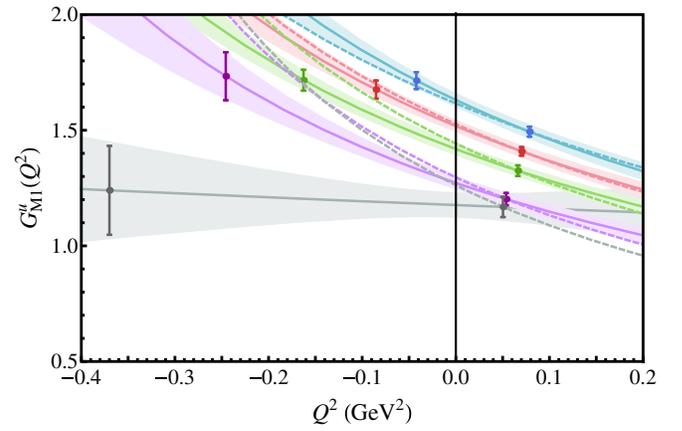

FIG. 6 (color online).   Quark sector results for the transition form factor, G_{M1}^u. Each curve corresponds to a different value of m_π, with the top curve (blue) corresponding to the heaviest and masses getting lighter as we move down. For each mass we have access to two values of Q^2 stemming from the freedom to choose which hadron is as rest. The solid line and colored bands are the resulting monopole parametrization extracted from the two data points, allowing us to access $G_{M1}(0)$. We also include a VMD estimate, dashed line, obtained from using the right positive Q^2 data only, with ρ-meson mass used as the monopole mass Λ.

$G_{M1}^u(0)$, we compare our results with the VMD estimate obtained using spacelike data and the rho meson mass as the monopole mass. This result is shown as the dashed line in Fig. 6. In Fig. 7 we show the monopole masses extracted from our analysis. We also include the corresponding rho meson masses and find that they compare reasonably well at large quark masses, but diverge in the light-quark regime. Indeed, at the lightest mass $\Lambda \simeq 0$. This draws the monopole ansatz into question deep in the timelike regime. Thus
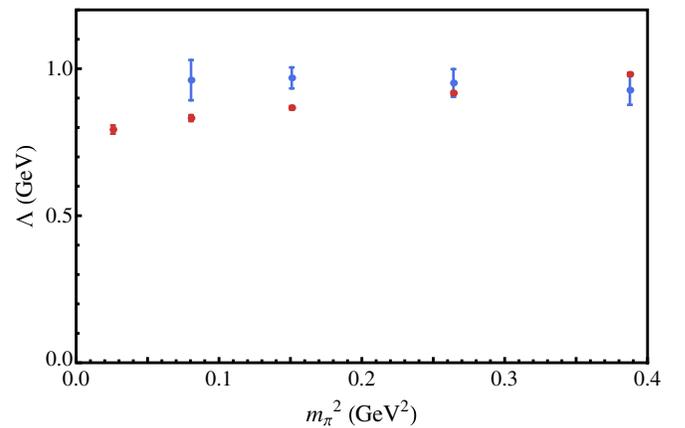

FIG. 7 (color online).   Monopole mass, Λ, (blue) obtained from applying monopole ansatz to the data. The corresponding ρ-meson mass (red) is included to test the VMD hypothesis. The monopole mass for the lightest quark mass is not included due to the large uncertainty in Λ^2 stemming from the similar values for $G_{M1}^u(Q_1^2)$ and $G_{M1}^u(Q_2^2)$.

to connect to experiment we also work with results in the spacelike regime ($Q^2 > 0$) and employ VMD.

We now consider the full hadronic transition form factor. As was noted earlier, for this transition the quark and antiquark sector contributions are of equal magnitude and opposite sign and so the charge weighted form factor for $\rho^+ \to \pi^+\gamma$ is given by

$$G_{M1}(Q^2) = \frac{2}{3}G_{M1}^u(Q^2) + \frac{1}{3}(-G_{M1}^u(Q^2))$$
$$= \frac{1}{3}G_{M1}^u(Q^2).$$

Table I summarizes our lattice results. In Fig. 8 we present our results for $G_{M1}(0)$. We also include the nonrelativistic quark model expectation [36] and the available experimental data. Due to the different choice of normalization for this matrix element, we match conventions via the decay width. The relevant expression for the decay width using our choice of normalization [5] is

$$\Gamma_{\rho\to\pi\gamma} = \frac{1}{3}\alpha\frac{|\vec{q}|^3}{m_\rho^2}|G_{M1}(0)|^2, \qquad (10)$$

where the photon 3-momentum is evaluated in the rest frame for ρ meson

$$|\vec{q}| = \frac{m_\rho^2 - m_\pi^2}{2m_\rho}.$$

Using this expression we are able to evaluate $G_{M1}(0)$ for experimental measurements of the decay width. We include the PDG average [1] as well as the three experimental measurements [37–39] used in its evaluation. For the quark model, the choice of normalization used in Ref. [36] results in the following expression for the decay width

$$\Gamma_{\rho\to\pi\gamma} = \frac{2}{3}\alpha|\vec{q}|^3\left(\frac{E_\pi}{m_\rho}\right)\sum_q\left|\langle\rho|\frac{\mu_q e_q \sigma_q}{e}|\pi\rangle\right|^2.$$

TABLE I. Lattice results for the charge-weighted form factor G_{M1} of $\rho^+ \to \pi^+\gamma$ for the two available Q^2-values for each pion mass.

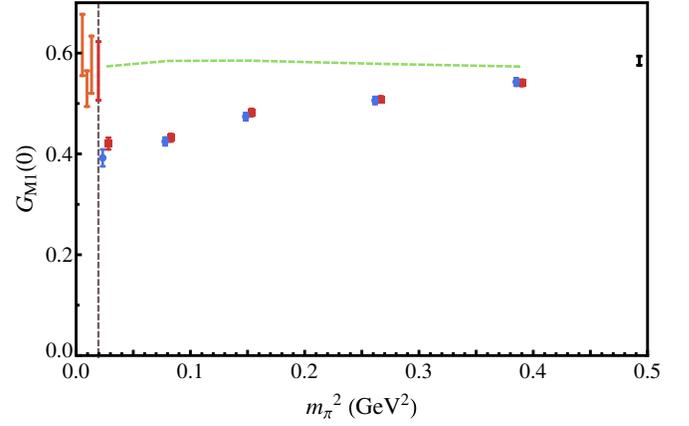| κ	m_π (GeV)	m_ρ (GeV)	Q^2 (GeV^2)	$G_{M1}(Q^2)$
13700	0.6226(9)	0.981(5)	−0.042(5)	0.572(12)
			0.078(3)	0.498(7)
13727	0.5145(9)	0.917(6)	−0.085(5)	0.559(13)
			0.070(3)	0.470(6)
13754	0.3884(9)	0.867(6)	−0.163(6)	0.572(15)
			0.066(3)	0.442(8)
13770	0.2848(11)	0.832(10)	−0.246(10)	0.578(35)
			0.054(6)	0.401(9)
13781	0.1613(31)	0.793(14)	−0.370(17)	0.413(64)
			0.050(9)	0.389(15)

FIG. 8 (color online). Results for the full hadronic transition moment, $G_{M1}(0)$, extracted using both space and timelike Q^2 values (blue circles) and using the spacelike values only and invoking the VMD hypothesis (red squares). We include the available experimental extractions (orange) ordered from left to right by year of publication [37–39]. We also include the PDG average (red) obtained from this data [1]. The experimental data are offset for readability, with the PDG average aligned at the physical point indicated by the vertical dashed line. The dashed green line is the nonrelativistic quark model expectation of Ref. [36] as discussed herein. We also include the result of Shultz *et al.* [9] (black) which determines this moment for a single heavy-quark mass.

As discussed in Ref. [36], by using SU(6) quark and antiquark flavor combinations, the sum evaluates to

$$\sum_q\left|\langle\rho|\frac{\mu_q e_q \sigma_q}{e}|\pi\rangle\right|^2 = \frac{2}{9}\frac{\mu_{ud}^2}{e^2},$$

where the light-quark magnetic moment is

$$\mu_{ud} = \frac{e}{2m_{ud}}.$$

Matching with Eq. (10), this gives rise to the following expression

$$G_{M1}(0) = \frac{2}{3}\sqrt{m_\rho E_\pi}\frac{\mu_{ud}}{e}.$$

For the quark moment, μ_{ud}, we use a constituent quark mass that varies linearly in m_π^2

$$m_{ud} = a + bm_\pi^2,$$

with a and b fixed such that the constituent quark has a mass of 330 MeV at the physical point and 510 MeV at the SU(3) symmetric point, as determined in Ref. [1] using the magnetic moments μ_p, μ_n and μ_Λ.

Beginning with our results at the heaviest values of m_π, we find that our lattice data is close to the quark model expectation. Furthermore the observed trend in the data suggests consistency with increasing quark mass where we

would expect the quark model expectation to hold. The trend in the data also appears consistent with the determination of Ref. [9]. As we move down to the lighter masses there is a clear downwards trend in the lattice data, as was also observed in our previous quenched study [7,40] In contrast to this the quark model result shows little variation with varying m_π. In the light-quark regime, we do not expect the quark model to necessarily hold for this transition. Unlike heavier systems such as bottomium and charmonium decays, the quarks in both the pi and rho meson systems are highly relativistic. Furthermore, the pion itself is a goldstone mode of QCD stemming from the underlying chiral symmetry of the theory. Though we can in principle treat the quarks relativistically [41,42], the inability to properly describe the chiral behavior of the pion is a fundamental shortfall of all constituent quark models and may certainly lead to deviations in the chiral limit.

Comparison with the experimental determination shows a notable deviation, with the lattice data sitting around 33% lower than the experimental value. In Fig. 8 we also include the values obtained using VMD with the spacelike data only and find that significant differences persist. However, we note that our calculation is incomplete. Unlike the elastic form factors for which disconnected contributions are necessarily zero [15,31], such contributions are present for meson transitions that involve a change in G-parity [9]. This is related to the invariance of the QCD action under charge-conjugation. For disconnected contributions involving the electromagnetic current, under charge-conjugation the "C-even" two-point function and the "C-odd" disconnected loop give rise to a relative sign between the $\{U\}$ and $\{U^*\}$ configurations and so cancel exactly [31] in the ensemble average. For transitions involving a change in G-parity, the two-point function is now "C-odd" and so combining with the disconnected loop gives rise to a common sign between the $\{U\}$ and $\{U^*\}$ configurations resulting in a nonzero quantity [9,15]. Furthermore, if one neglects disconnected s-quark contributions, the charge weight factors between the connected contributions and the disconnected contributions are equal

$$
\begin{aligned}
G_{M1} &= q_u G_{M1}^{\text{con}} + q_{\bar{d}}(-G_{M1}^{\text{con}}) + q_u G_{M1}^{\text{dis}} + q_d G_{M1}^{\text{dis}} \\
&= \left(\frac{2}{3} - \frac{1}{3}\right) G_{M1}^{\text{con}} + \left(\frac{2}{3} - \frac{1}{3}\right) G_{M1}^{\text{dis}} \\
&= \frac{1}{3} G_{M1}^{\text{con}} + \frac{1}{3} G_{M1}^{\text{dis}}.
\end{aligned}
$$

Thus the discrepancy between our results and the experimental value suggest that disconnected contributions are likely to play an important role in fully describing this transition. One would also expect such contributions to become increasing important with decreasing quark mass. This expectation complements the observation that our results are consistent with quark model expectations at

heavier masses and deviate as we move to light-quark regime.

Another important aspect that warrants further consideration is the fact that the rho meson is ultimately a resonant state. The nature of resonant states on the lattice is significantly different to that of continuum due to the lack of a continuous distribution of momentum modes and so to properly make connection with the continuum expectation, one must suitably evolve the lattice determinations to the infinite volume to properly account for the differences in the underlying multiparticle interactions. Understanding exactly how to do this in general is an area of current interest to the community and only very recently has a framework been presented to handle $1 \to 2$ body processes required to properly describe this transition [43–45]. In fully addressing this aspect, it is important to also consider the role of $\pi\pi$ scattering states in the ρ-meson correlation matrix to ensure a complete isolation of QCD eigenstates on the finite volume.

VI. CONCLUDING REMARKS

In this work we present the first light-quark examination of the radiative decay of the rho meson. The calculated transition moment, $G_{M1}(0)$, was found to be consistent with quark model expectations at heavy masses. However, we have discovered an important quark mass dependence. Our results in the light-quark regime sit low in comparison with experimental determinations, suggesting important disconnected contributions to this process.

These results warrant a more comprehensive investigation of this process. Any future work should aim to focus on the inclusion of disconnected contributions, multiparticle contributions and finite volume effects so as to allow for the proper evolution of the lattice determination to the infinite volume. Understanding the role these systematics play in this calculation may provide important insights into topical transition amplitudes such as $N^* \to N\gamma^*$ and $\Delta^{(*)} \to N\gamma^*$ transitions and those central to the search for exotic hadron states [4].

[1] K. Olive *et al.* (Particle Data Group), Chin. Phys. C **38**, 090001 (2014).

[2] C. Thomas, *Proc. Sci.*, LATTICE2014 (2014) 003.

[3] J. Bulava, *Proc. Sci.*, LATTICE2011 (2011) 021 [arXiv:1112.0212].

[4] J. Dudek, R. Ent, R. Essig, K. Kumar, C. Meyer *et al.*, Eur. Phys. J. A **48**, 187 (2012).

[5] R. Woloshyn, Z. Phys. C **33**, 121 (1986).

[6] M. Crisafulli and V. Lubicz, Phys. Lett. B **278**, 323 (1992).

[7] B. Owen, W. Kamleh, D. Leinweber, A. El Bakry, and P. Moran, *Proc. Sci.*, LATTICE2012 (2012) 254.

[8] R. G. Edwards (Lattice Hadron Physics), Nucl. Phys. B, Proc. Suppl. **140**, 290 (2005).

[9] C. J. Shultz, J. J. Dudek, and R. G. Edwards, Phys. Rev. D **91**, 114501 (2015).

[10] S. Dinter, C. Alexandrou, M. Constantinou, V. Drach, K. Jansen, and D. B. Renner, Phys. Lett. B **704**, 89 (2011).

[11] H.-W. Lin, *Proc. Sci.*, LATTICE2012 (2012) 013 [arXiv:1212.6849].

[12] C. Alexandrou, *Proc. Sci.*, LATTICE2010 (2010) 001 [arXiv:1011.3660].

[13] B. J. Owen, J. Dragos, W. Kamleh, D. B. Leinweber, M. S. Mahbub, B. J. Menadue, and J. M. Zanotti, Phys. Lett. B **723**, 217 (2013).

[14] B. Owen, W. Kamleh, D. Leinweber, B. Menadue, and S. Mahbub, Phys. Rev. D **91**, 074503 (2015).

[15] J. J. Dudek, R. G. Edwards, and D. G. Richards, Phys. Rev. D **73**, 074507 (2006).

[16] J. J. Dudek, R. Edwards, and C. E. Thomas, Phys. Rev. D **79**, 094504 (2009).

[17] J. Bulava, M. Donnellan, and R. Sommer, J. High Energy Phys. 01 (2012) 140.

[18] R. Lewis and R. Woloshyn, Phys. Rev. D **84**, 094501 (2011).

[19] T. Maurer, T. Burch, L. Y. Glozman, C. Lang, D. Mohler *et al.*, arXiv:1202.2834.

[20] B. Blossier, J. Bulava, M. Donnellan, and A. Grardin, Phys. Rev. D **87**, 094518 (2013).

[21] C. Michael, Nucl. Phys. **B259**, 58 (1985).

[22] M. Luscher and U. Wolff, Nucl. Phys. **B339**, 222 (1990).

[23] J. N. Hedditch, W. Kamleh, B. G. Lasscock, D. B. Leinweber, A. G. Williams, and J. M. Zanotti, Phys. Rev. D **75**, 094504 (2007).

[24] C. Bernard, T. Draper, G. Hockney, and A. Soni, in *Lattice Gauge Theory: A Challenge in Large-Scale Computing,*

NATO Science Series B, edited by B. Bunk, K. H. Mutter, and K. Schilling (Springer, New York, 1986).

[25] C. Bernard, in *Gauge Theory on A Lattice: 1984: Proceedings of the Argonne National Laboratory Workshop*, edited by C. K. Zachos, E. Kovacs, D. W. Sivers, and W. Celmaster (Argonne National Laboratory, Argonne, IL, 1984).

[26] S. Boinepalli, D. Leinweber, A. Williams, J. Zanotti, and J. Zhang, Phys. Rev. D **74**, 093005 (2006).

[27] T. Draper, R. Woloshyn, W. Wilcox, and K.-F. Liu, Nucl. Phys. B, Proc. Suppl. **9**, 175 (1989).

[28] S. Aoki *et al.*, Phys. Rev. D **79**, 034503 (2009).

[29] M. G. Beckett, P. Coddington, B. Joó, C. M. Maynard, D. Pleiter, O. Tatebe, and T. Yoshie, Comput. Phys. Commun. **182**, 1208 (2011).

[30] R. Sommer, Nucl. Phys. **B411**, 839 (1994).

[31] T. Draper, R. Woloshyn, W. Wilcox, and K.-F. Liu, Nucl. Phys. **B318**, 319 (1989).

[32] G. Martinelli, C. T. Sachrajda, and A. Vladikas, Nucl. Phys. **B358**, 212 (1991).

[33] M. S. Mahbub, W. Kamleh, D. B. Leinweber, P. J. Moran, and A. G. Williams (CSSM Lattice), Phys. Lett. B **707**, 389 (2012).

[34] D. S. Roberts, W. Kamleh, and D. B. Leinweber, Phys. Rev. D **89**, 074501 (2014).

[35] M. S. Mahbub, W. Kamleh, D. B. Leinweber, and A. G. Williams, Ann. Phys. (N.Y.) **342**, 270 (2014).

[36] P. J. O'Donnell, Rev. Mod. Phys. **53**, 673 (1981).

[37] T. Jensen, D. Berg, C. Chandlee, S. Cihangir, T. Ferbel *et al.*, Phys. Rev. D **27**, 26 (1983).

[38] J. Huston, D. Berg, C. Chandlee, S. Cihangir, B. Collick *et al.*, Phys. Rev. D **33**, 3199 (1986).

[39] L. Capraro, P. Levy, M. Querrou, B. Van Hecke, M. Verbeken *et al.*, Nucl. Phys. **B288**, 659 (1987).

[40] We note that in this proceedings, there was an error in converting the experimental decay widths to our definition of the form factor $G_{M1}(0)$. The lattice data, however, is correct and consistent with results presented herein. Comparison with experiment for [7] should be done with the value presented here.

[41] N. Barik, P. Dash, and A. Panda, Phys. Rev. D **46**, 3856 (1992).

[42] N. Barik and P. Dash, Phys. Rev. D **49**, 299 (1994).

[43] V. Bernard, D. Hoja, U. Meissner, and A. Rusetsky, J. High Energy Phys. 09 (2012) 023.

[44] A. Agadjanov, V. Bernard, U.-G. Meiner, and A. Rusetsky, Nucl. Phys. **B886**, 1199 (2014).

[45] R. A. Briceo, M. T. Hansen, and A. Walker-Loud, Phys. Rev. D **91**, 034501 (2015).